



HAL
open science

Enhancement of the photocatalytic activity of decatungstate, W₁₀O₃₂⁴⁻, for the oxidation of sulfasalazine/sulfapyridine in the presence of hydrogen peroxide

P. Cheng, Yajie Wang, M. Sarakha, Gilles Mailhot

► **To cite this version:**

P. Cheng, Yajie Wang, M. Sarakha, Gilles Mailhot. Enhancement of the photocatalytic activity of decatungstate, W₁₀O₃₂⁴⁻, for the oxidation of sulfasalazine/sulfapyridine in the presence of hydrogen peroxide. *Journal of Photochemistry and Photobiology A: Chemistry*, 2021, 404, pp.112890. 10.1016/j.jphotochem.2020.112890 . hal-03052327

HAL Id: hal-03052327

<https://uca.hal.science/hal-03052327>

Submitted on 10 Dec 2020

HAL is a multi-disciplinary open access archive for the deposit and dissemination of scientific research documents, whether they are published or not. The documents may come from teaching and research institutions in France or abroad, or from public or private research centers.

L'archive ouverte pluridisciplinaire **HAL**, est destinée au dépôt et à la diffusion de documents scientifiques de niveau recherche, publiés ou non, émanant des établissements d'enseignement et de recherche français ou étrangers, des laboratoires publics ou privés.



Distributed under a Creative Commons Attribution 4.0 International License

1 **Enhancement of the photocatalytic activity of Decatungstate, $W_{10}O_{32}^{4-}$,**
2 **for the oxidation of sulfasalazine/sulfapyridine in the presence of**
3 **hydrogen peroxide**

4
5 P. Cheng¹, Yajie Wang², M. Sarakha^{1*}, G. Mailhot¹
6

7 ¹Université Clermont Auvergne, CNRS, Sigma Clermont, Institut de Chimie de Clermont Ferrand
8 (ICCF) UMR 6296, BP 80026, F-63171, Aubière cedex, France.

9 ²School of Eco-Environmental Engineering, Guizhou Minzu University, Guiyang 550025, China

10 * **Corresponding author**

11
12 **Abstract**

13 The degradations of sulfasalazine and also sulfapyridine have been investigated by using the
14 sodium decatungstate $Na_4W_{10}O_{32}$ as a photocatalyst in the presence of hydrogen peroxide as a
15 sacrificial agent. The selective irradiation of decatungstate, $W_{10}O_{32}^{4-}$, in the presence of the pollutants
16 at 365 nm and at pH = 4.0 leads to the reduction of hydrogen peroxide via a Fenton like reaction
17 involving the reduced species, $W_{10}O_{32}^{5-}$. Such process represents an efficient way for the formation
18 of the highly reactive species, namely the hydroxyl radicals. The process appears then to be highly
19 efficient for the oxidation of the pollutants sulfasalazine and sulfapyridine. Under our experimental
20 conditions, the process was optimized in terms of concentrations of the photocatalyst, hydrogen
21 peroxide and pollutant concentrations and also in term of pH. For both pollutants, the analysis of the
22 generated by-products, using HPLC/MS, shows that the degradation proceeds primarily through
23 three and common chemical processes: i) hydroxylation ii) desulfurization and iii) scission at the azo
24 group -N=N-. The attack of the hydroxyl radical is clearly the main species for the degradation
25 processes. As clearly demonstrated by the TOC experiments, the combination of $W_{10}O_{32}^{4-}/H_2O_2/h\nu$
26 system permitted a total mineralization of the solution indicating its high efficiency for the a
27 potential application of water depollution.
28

1. Introduction

Nowadays, the emergence of antibiotics in the environment and their potential hazards have attracted more and more attention [1-3]. Most antibiotics are not completely absorbed by the body, and an average of more than 50-90% of the antibiotics are excreted in the form of protoplasts or metabolites, which have been widely detected in surface water, groundwater, sewage treatment plant effluent, drinking water and soil sediments [4]. For example, antibiotics such as ofloxacin at 306 ng L⁻¹, lincomycin at 249 ng L⁻¹ and spiramycin at 74 ng L⁻¹ and trace amounts of amoxicillin and penicillin were detected in the Lambro and Po rivers in Italy at significant concentrations [5]. The presence of antibiotics into the environment not only has adverse effects on the ecosystem, such as the emergence of resistant pathogens and toxicity to aquatic organisms, but also can enter the human body through the enrichment of food chain, leading to a serious threat to human health such as causing vomiting or diabetes mellitus [6, 7]. The common occurrence of abusing of antibiotics is easily found especially in aquaculture field in some Asian countries like China and India. China has been one of the largest producers and users of the antibiotics in the world, approximately 162 000 tons of antibiotics were used in 2013. Aquaculture consumption accounted for about 52% of the total antibiotics [8]. Therefore, the treatment of antibiotics in the environment is particularly important.

The biological, adsorption and chemical oxidation methods, etc. were applied in treating the antibiotics present in wastewater. For example, Xiong et al. combined amino-functionalized Metal-organic framework (MOFs, MIL-53(Fe)) with multi-walled carbon nanotubes (MWCNT) to synthesize a novel adsorbent composite which was used to adsorb tetracycline hydrochloride (TCN) and chlortetracycline hydrochloride (CTC) [9]. While antibiotics are composed by various functional groups and substituents, the structure is very different, which makes the adsorption behavior on adsorbents different for distinct antibiotics and so the efficiency of the treatment will be strongly chemical structure dependent.

Advanced oxidation processes (AOPs), also known as deep oxidation technology, are characterized by the generation of reactive species (reactive oxygen species "ROS"), such as hydroxyl radicals (HO[•]), sulfate radicals (SO₄^{•-}), with strong oxidizing power [10]. The organic substances which are difficult to degrade, can be oxidized into a low-toxic or non-toxic small molecule substance, and very often more readily (bio-)degradable, [4, 11-15]. Due to its green environmentally friendly sustainable properties, the photocatalytic oxidation became one of the best

59 promising techniques in treating organic wastewater. Many researchers develop important energy in
60 the synthesis of new photocatalysts or the modification of already prepared photocatalyst with the
61 aim to improve the efficiency of organic pollutants degradation.

62 The decatungstate anion ($W_{10}O_{32}^{4-}$) was shown to be one of the most photo-chemically active
63 polyoxometalates, which catching the interesting of thousands of researchers over the past 30 years
64 [16]. It is worth noting that $W_{10}O_{32}^{4-}$ absorbs in the UV with a maximum at 320 nm and its
65 absorption spectrum presents a useful overlap with the solar emission spectrum. Illumination of
66 $W_{10}O_{32}^{4-}$, within the range 300 - 400 nm, leads to the formation of an oxygen-to-metal charge
67 transfer excited state $W_{10}O_{32}^{4-*}$ that decays in less than 30 ps to an extremely reactive non-emissive
68 transient, which has been referred to as wO [17]. This latter species is able to oxidize organic
69 compounds through electron transfer or/and hydrogen abstraction owing to the presence of an
70 electron-deficient oxygen center. In decatungstate system, the reactive species has a lifetime τ_{wO} of
71 65 ± 5 ns in the case of sodium decatungstate and its formation quantum yield Φ_{wO} is 0.57 [17]. Such
72 reaction between wO and appropriate hydrogen or/and electron donor leads to the formation of the
73 one electron reduced form of decatungstate $W_{10}O_{32}^{5-}$ that absorbs in the visible region with a
74 maximum at 778 nm. The reduction of molecular oxygen to superoxide anion by such species is an
75 efficient process for the regeneration of the starting catalyst, $W_{10}O_{32}^{4-}$. In previous studies, the
76 decatungstate ($W_{10}O_{32}^{4-}$) was used as an efficient and optimistic tool in organic synthesis, which can
77 functionalize some organic compounds such as alkanes, alkenes, alcohols, aldehydes and sulfides in
78 organic and aqueous media via free radical carbon-centered intermediates [18]. On the other hand,
79 the decatungstate was also deeply studied for water depollution. Allaoui et al. studied the
80 photodegradation of 2-mercaptobenzothiazole (MBT) and illustrated that the photodegradation rate
81 of MBT clearly increased in the presence of decatungstate ($W_{10}O_{32}^{4-}$) by a factor of six when
82 compared with the direct photolysis; and oxygen appeared to be the key species for catalyst
83 regeneration [19].

84 In the present work, we choose the soluble sodium decatungstate ($Na_4W_{10}O_{32}$) as a
85 photocatalyst to degrade the sulfonamides antibiotics (sulfasalazine and sulfapyridine). Moreover,
86 and in this homogeneous system, we added hydrogen peroxide as a supplementary oxidant (with
87 oxygen) in order to oxidize the reduced species of decatungstate ($W_{10}O_{32}^{5-}$) permitting the efficient

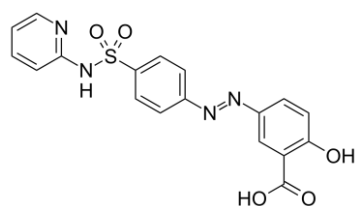
88 regeneration of the starting $W_{10}O_{32}^{4-}$. This additional process permits the formation of the highly
89 reactive species, namely hydroxyl radicals. Our purpose was to evaluate the photodegradation of
90 sulfasalazine (SSZ) and sulfapyridine (SPD) through the determination of kinetics, the initial rate
91 constants and the yields of SSZ and SPD degradation. In addition, with the photoproducts
92 identification, the mechanistic pathways involved in the degradation will be proposed with the aim to
93 have a better insight into the SSZ and SPD degradation scheme.

94

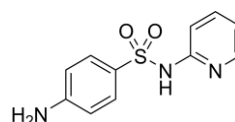
95 **2. Materials and Methods**

96 **2.1. Materials**

97 Sulfasalazine (SSZ) (99.8%), Sulfapyridine (SPD) ($\geq 99\%$), sodium tungstate ($Na_2WO_4 \cdot 2H_2O$),
98 sodium chloride (NaCl), hydrochloric acid (HCl), hydroperoxide (H_2O_2), perchloric acid ($HClO_4$),
99 and sodium hydroxide (NaOH) were purchased from Sigma Aldrich and used as received. Water was
100 purified using a reverse osmosis RIOS 5 and Synergy (Millipore) device (resistivity $18 M\Omega \cdot cm$,
101 $DOC < 0.1 mg \cdot L^{-1}$).



102
103 **SSZ**



104
105 **SPD**

106

107 **2.2. Preparation and characterization of sodium decatungstate**

108 The preparation of sodium decatungstate refers to the previous studies available [20]. The
109 boiling sodium tungstate solution (50 g of $Na_2WO_4 \cdot 2H_2O$ dissolved in 300 mL of ultrapure water)
110 was mixed with 1.0 M boiling hydrochloric acid (300 mL) in a beaker, refluxed for 20 seconds to
111 form a green solution. It was followed by adding 150 g of solid sodium chloride, stirring until the
112 solution has been re-boiled and keeping for 20 seconds, then rapidly putting into the ice-water bath.
113 This suspension solution was maintained in a freezer ($-18^\circ C$) overnight. The next day, this
114 suspension solution of NaCl and crude $Na_4W_{10}O_{32}$ was filtered and the solid was dissolved into 150
mL of acetonitrile solution. The acetonitrile solution was refluxed for 5 min at $79^\circ C$ and filtered to
remove the insoluble NaCl after cooling at ambient temperature. The acetonitrile solution was gently

115 evaporated in hot-water bath (79°C) to obtain the yellow-green catalyst.

116 The UV-Vis absorption spectra were obtained using a Varian Cary 300 UV-visible
117 spectrophotometer. The infrared absorption spectra were obtained by Fourier infrared absorption
118 spectrometer, operated by potassium bromide pressed-disk technique (98% KBr).

119 **2.3 Irradiation experiments and photoreactor**

120 Irradiation experiments (365 nm) were carried out in a stainless-steel cylindrical reactor. Six
121 high pressure mercury lamps (Philips HPW, 15W, emission centered at 365 nm) was located evenly
122 on the edge of the cylinder with a fan placed on the bottom of the cylinder to cool the irradiation
123 system. The reactor, a Pyrex tube (2 cm diameter), was placed at the center of the cylinder (**Figure**
124 **S1**).

125 The degradation of SSZ and SPD was performed in a batch experiment. The 5.0×10^{-5} M
126 solution of SSZ and SPD was prepared and 10.0 mg soluble decatungstate was added into the 100
127 mL of SSZ or SPD solution, the concentration of decatungstate was then evaluated to 4.0×10^{-5} M.
128 Hydrogen peroxide was added using a concentrated solution, and so with negligible volume, prior to
129 irradiation using the photo-reactor system. The pH of solution was adjusted to 4.0 ± 0.05 using
130 perchloric acid and sodium hydroxide (0.1 M). Aliquots were taken at different interval times of 0, 2,
131 5, 10, 15, 20, 25 min at ambient temperature.

132 The effect of initial pH was studied at 23 °C using a similar procedure, 10 mg decatungstate
133 (4.0×10^{-5} M) were mixed with 100 mL 5.0×10^{-5} M solution of SSZ or SPD at different initial pH of 3,
134 4, 5 and 6. The solution pHs were adjusted by adding small negligible volume of perchloric acid
135 and/or sodium hydroxide (0.1 M).

136 The effect of the concentration of H_2O_2 (from 10^{-5} to 10^{-2} M), SSZ and SPD (5.0×10^{-6} , 10^{-5} ,
137 2.0×10^{-5} , 5.0×10^{-5} and 1.0×10^{-4} M) and decatungstate (2.0×10^{-5} , 4.0×10^{-5} , 7.0×10^{-5} , 1.0×10^{-4} and
138 2.0×10^{-4} M) were also investigated.

139 **2.4 HPLC Analysis**

140 The concentrations of SSZ and SPD were evaluated by HPLC (Shimadzu NEXERA XR HPL)
141 equipped with a photodiode array detector and an auto sampler. The column was a Macherey Nagel
142 EC 150/2 NUCLEODUR C18ec (150 mm \times 2 mm, 2 μ m particle size)

143 The analysis of SSZ was performed using methanol (MeOH, solvent B) as mobile phase and

144 water with 0.5 % phosphoric acid (solvent A) at a flow rate of 0.20 mL min⁻¹. The elution was
145 performed using the following gradient: 40 % of B for 5min, linear increase of B to 95 % in 15 min,
146 95 % of B for 5 min and decrease of B to 40 % in 0.1 min. For SPD, the analyses were performed
147 using acetonitrile (ACN, solvent C) as mobile phase and water with 0.5 % of phosphoric acid at a
148 flow rate of 0.40 mL min⁻¹. The elution was performed using the following gradient: 5 % of C for 2.5
149 min, linear increase of C to 40 % in 4.5 min, then increase of C to 95 % in 1.5 min, 95 % of C for 1
150 min and decrease of C to 5 % in 0.5 min.

151 The identification of degradation products was performed using high resolution mass
152 spectrometry (HRMS) constituted of an Orbitrap Q-Exactive (ThermoScientific) coupled to an
153 ultra-high performance liquid chromatography (UHPLC) instrument Ultimate 3000 RSLC
154 (ThermoScientific). Analyses were carried out in both negative and positive electrospray modes
155 (ESI⁺ and ESI⁻). SSZ, SPD and the degradation products were separated using the same elution
156 gradient as previously indicated. The column was a Kinetec EVO C18 Phenomenex (100 mm × 2.1
157 mm, particle size of 1.7 μm) and the flow rate was set at 0.45 mL·min⁻¹.

158 **2.5 TOC Analysis**

159 The concentration of the total organic carbon (TOC) in the aqueous solution was followed on a
160 Shimadzu TOC 5050A analyzer. The TOC value was the average of three individual injections.

161

162 **3. Results**

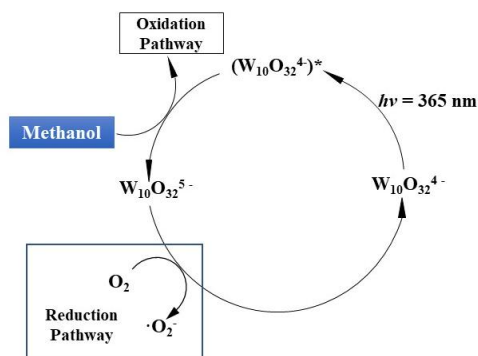
163

164 **3.1. Characterization and photochemistry behavior of the photocatalyst**

165 The UV-visible spectrum of the synthesized photocatalyst decatungstate, W₁₀O₃₂⁴⁻ (**W**), is given
166 in **Figure 1**. It shows an absorption band with a defined maximum at 321 nm and a molar absorption
167 coefficient of 12365 M⁻¹ cm⁻¹ in perfect agreement with the published literature data [20]. The UV
168 absorption extends up to 400 nm indicating an important and interesting overlap with the emission
169 spectrum of solar light. In addition to the UV visible spectrum, the characterization of the
170 decatungstate was also performed by employing the Fourier transformed IR. In **Figure S2**, the strong
171 broad band centered at around 3500 cm⁻¹ and the peak at around 1600 cm⁻¹ are attributed to the O–H

172 stretching vibrations and to the bending modes of water molecules. This implied that the
173 hydrophilicity of the substrate will improve the photocatalysis activity as suggested by H-Y. He [21,
174 22]. The main vibration bands of decatungstate ($W_{10}O_{32}^{4-}$) are observed at 1006 cm^{-1} corresponding
175 to the stretching vibration of the W=O bond, and at 962, 915, 796, 667, 586, 431 cm^{-1} due to the
176 deformation of W-O-W bonds [17, 23, 24]. Moreover, and as largely reported in the literature [16, 25,
177 26], the excitation of the mixture decatungstate and methanol (used as a sacrificial agent since it acts
178 as an electron or/and hydrogen donor) permits in deoxygenated conditions the formation of a blue
179 component that presents two well defined bands with maximums at 360 and 780 nm (**Figure S3**)
180 with roughly similar molar absorption coefficients ($6.7\text{-}6.9 \times 10^3\text{ M}^{-1}\text{ cm}^{-1}$ at 360 nm and $9.5\text{-}11 \times$
181 $10^3\text{ M}^{-1}\text{ cm}^{-1}$ at 780 nm). Such absorptions are owing to the formation of the reduced species of
182 decatungstate, namely $W_{10}O_{32}^{5-}$ that disappears rapidly by bubbling oxygen through an electron
183 transfer process leading to the formation of superoxide anion radical $O_2^{\bullet-}$ with the simultaneous
184 regeneration of the starting photocatalyst decatungstate [27] (**Scheme 1**). Such interesting behavior
185 was used within the present work to enhance the ability of the photocatalyst to decontaminate
186 polluted waters by producing reactive oxygen species (ROS) that are highly oxidant such as hydroxyl
187 radical. The formation of this latter species was reached by introducing hydrogen peroxide as a
188 sacrificial reactant.

189



190

191

192 **Scheme 1:** Photocatalytic cycle of decatungstate upon UV excitation in the presence of methanol
 193 showing oxidation and reduction processes.

194

195 The efficiency of the photocatalytic cycle was studied and optimized by studying sulfonamides
 196 antibiotics sulfasalazine (SSZ) and sulfapyridine (SPD) degradations.

197

198 **3.2. Degradation of SSZ and SPD by decatungstate, H₂O₂ or decatungstate/H₂O₂ systems under**
 199 **UVA irradiation**

200 In order to evaluate the efficiency of the decatungstate photocatalysis process, irradiations were
 201 performed under UVA (365 nm) for different aerated solutions in the presence of SSZ in various
 202 conditions (SSZ alone, SSZ + H₂O₂, SSZ + W and SSZ + H₂O₂ + W). As clearly shown in **Figure 2A**,
 203 no degradation was noted when SSZ was alone in aqueous solution, despite its significant absorption
 204 at the excitation wavelength. This indicates the relative photochemical stability of SSZ under our
 205 experimental conditions. However, in the presence of hydrogen peroxide, a negligible degradation
 206 was observed representing 2% within 120 minutes of irradiation. In the presence of decatungstate,
 207 the conversion percentage of SSZ reached 16% demonstrating the oxidation ability of the
 208 photocatalyst decatungstate through an oxidation process (electron transfer) as shown in **Scheme 1**.
 209 The initial rate of SSZ disappearance was estimated to $1.2 \times 10^{-7} \text{ M min}^{-1}$. By addition of hydrogen
 210 peroxide in the previous system, the conversion percentage increased significantly in agreement with
 211 the fact that hydrogen peroxide interacts in the photocatalytic cycle and presents a positive and
 212 beneficial effect when it is used simultaneously with decatungstate. In this latter system, the
 213 degradation of SSZ reaches 28% after 120 minutes irradiation time with an initial rate of $1.6 \times 10^{-7} \text{ M}$

214 min⁻¹. The benefit of hydrogen peroxide in the photocatalysis process is then effective and it was
215 deeply studied and optimized within the present work. Similar experiments were performed with
216 SPD showing a more pronounced degradation. This is owing to the fact that SPD does not absorb at
217 the excitation wavelength, in contrary to SSZ, and thus no competition of the absorbed light intensity
218 is involved (**Figure 2B**). The initial rate of SPD degradation was estimated to 4.3×10⁻⁷ M min⁻¹ and
219 7.0×10⁻⁷ M min⁻¹ in the presence of decatungstate and decatungstate/H₂O₂ respectively.

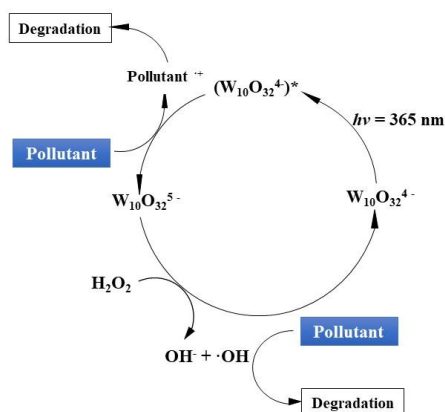
220 The involvement of hydrogen peroxide in the photocatalytic system was also studied by
221 analyzing its reactivity with the reduced species of decatungstate, namely W₁₀O₃₂⁵⁻. As shown in
222 **Scheme 1**, the latter species was selectively formed by irradiation of **decatungstate** (40 μM) in the
223 presence of 1 % of methanol in deaerated solution. W₁₀O₃₂⁵⁻ immediately disappears when hydrogen
224 peroxide is added to the solution with the regeneration of the W₁₀O₃₂⁴⁻. It is then clear that H₂O₂ is
225 efficiently reduced by W₁₀O₃₂⁵⁻ owing, very likely, to the following Fenton like process (**Equation**
226 **1**).



228 **Equation 1:** Fenton like reaction between W₁₀O₃₂⁵⁻ and H₂O₂.

229
230 The effective formation of hydroxyl radical as a reactive oxygen species (**ROS**) was
231 demonstrated by employing a probe such as terephthalic acid. As largely reported in the literature,
232 the reactivity of this non fluorescent substrate with hydroxyl radical leads to the formation of a
233 highly fluorescent hydroxyterephthalic acid [28]. As clearly shown in **Figure 3**, the excitation of
234 aerated aqueous solution of decatungstate (W) in the presence of terephthalic acid (TA) and
235 hydrogen peroxide (H₂O₂) at pH = 4.0 leads to a rapid and efficient formation of hydroxyterephthalic
236 acid (TAOH) from the early stages of the irradiation. This demonstrates the involvement of an
237 additional pathway for the formation of the reactive oxygen species, namely the hydroxyl radical.
238 The absence of the blue color following irradiation is a clear evidence for involvement of the reduced
239 species of decatungstate (W₁₀O₃₂⁵⁻) for the formation of this **ROS** species. The smaller amount of
240 hydroxyl radical in the absence of hydrogen peroxide could be due to the disproportionation process
241 of hydroperoxide radical and/or superoxide anion radical (HO₂[•]/O₂^{•-}) to form H₂O₂ [29]. It is then
242 clear from these results that the amount of hydroxyl radical mainly originates from the reactivity of

243 $W_{10}O_{32}^{5-}$ and hydrogen peroxide permitting the implication of a supplementary pathway for the
 244 degradation of the pollutants: first through the oxidation by the excited state of decatungstate via an
 245 electron transfer or/and hydrogen transfer processes and then through the oxidation by the hydroxyl
 246 radical generated via the Fenton like process (**Scheme 2**). It should be pointed out that the latter
 247 reaction is in competition with the reactivity of $W_{10}O_{32}^{5-}$ with oxygen.



248
 249 **Scheme 2:** Photocatalytic cycle of decatungstate in the presence of H_2O_2 showing the two ways for
 250 the organic pollutant degradation.

251
 252 In the following parts of the paper, the optimization of the experimental conditions was studied
 253 by analyzing the effect of various parameters such as: concentrations of decatungstate; hydrogen
 254 peroxide and organic pollutant and the initial pH of the solution. These parameters represent
 255 fundamental parameters for the photocatalysis to be effective since i) decatungstate is the absorbing
 256 species and thus its optimum concentration will insure high concentration of the excited state without
 257 the negative inner filter effect ii) hydrogen peroxide efficiently contributes in the system to the
 258 formation of hydroxyl radicals. The latter species react simultaneously with the pollutant and
 259 hydrogen peroxide via competitive reactions and iii) the stability of the photocatalyst depends on the
 260 solution pH.

261
 262 **3.3. Effect of different amount of decatungstate**

263 In order to study the effect of decatungstate concentration on the removal of the pollutants SSZ and
 264 SPD, the experiments were performed at $pH = 4.0$. As clearly shown in **Figure 4A and 4B**, the
 265 degradation rates of SSZ and SPD increase by increasing the concentration of the photocatalyst
 266 decatungstate. This effect is without any doubt due to the increase of the light absorption by

267 decatungstate at higher concentration. However, under our experimental conditions the degradation
268 rate rapidly levelled off when decatungstate concentration reaches 50 μM , as shown in **Figure 4C**.
269 This is more probably owing to the inner filter effect. Thus, the concentration close to 40 μM was
270 chosen as the optimal concentration of the photocatalyst for the following experiments.

271

272 **3.4. Effect of different concentrations of H_2O_2**

273 Table 1 gathers the initial degradation rate obtained for both pollutants by excitation of
274 decatungstate (40 μM) in the presence of various hydrogen peroxide concentrations. In the absence
275 of H_2O_2 and at lower concentration of H_2O_2 (1 mM), the disappearance initial rate is found roughly 4
276 times higher for SPD than for SSZ due to the absorption of light by SSZ. At higher concentrations of
277 H_2O_2 (10 to 100 mM), the disappearance initial rate of SPD is always higher than that of SSZ but by
278 a factor of about 1.5. In addition to the electron transfer between SSZ or SPD and $\text{W}_{10}\text{O}_{32}^{4-}$ excited
279 state, a second pathway is involved when hydrogen peroxide is added to the system via the
280 production of hydroxyl radicals as demonstrated above. As clearly shown in **Table 1**, this reaction is
281 effective despite the presence of dissolved molecular oxygen at a concentration of 2.6×10^{-4} M [30,
282 31]. Moreover, the initial disappearance rate increases when hydrogen peroxide concentration
283 increases. One should also note, that under our experimental conditions and at high concentrations,
284 the direct light absorption by hydrogen peroxide also participate in the generation of hydroxyl radical
285 and thus to the degradation of the pollutant through the homolytic scission of O-O bond [32, 33]. It
286 should be noted that at high concentration of hydrogen peroxide, the consumption of hydroxyl
287 radical could be observed by H_2O_2 itself which is detrimental under our experimental conditions [34,
288 35].

289

290 **3.5. Effect of different SSZ and SPD concentrations**

291 With the aim to use the photocatalyst decatungstate for various pollutants that have different
292 chemical structures and also different light absorption profiles, we undertook the effect of the
293 concentration of both pollutants, SSZ and SPD, on the efficiency of the photocatalytic process. We
294 can note that SPD does not absorb at the excitation wavelengths, namely at 365 nm, while SSZ
295 shows significant absorbance with a molar absorption coefficient $\epsilon_{365 \text{ nm}} = 21850.4 \text{ M}^{-1} \text{ cm}^{-1}$. The

296 experiments were performed by using decatungstate at the concentration of 40.0 μM in the presence
297 of H_2O_2 10 mM with various concentrations of the pollutants within the range 5.0 to 100 μM at
298 $\text{pH} = 4.0$. As shown in **Figure 5**, the initial disappearance rate of SPD increased by increasing its
299 initial concentration. This clearly shows that under our experimental conditions, hydroxyl radical is
300 involved in the oxidation of SPD but it is also trapped by hydrogen peroxide as largely reported in
301 the literature with a rate constant of $3.0 \times 10^7 \text{ M}^{-1} \text{ s}^{-1}$ [34, 35]. Such reaction is detrimental since it
302 participates to the decrease of the stationary concentration of the reactive species: hydroxyl radical.
303 So, the use of relatively high concentrations of SPD will be in favor of its degradation.

304 In the case of SSZ, the initial rate first increases within the concentration range 5.0 to 20.0 μM
305 and then decreases at higher concentrations. Such decrease of the initial rate is mainly owing to the
306 competition in the absorption of light intensity involving the photocatalyst decatungstate and SSZ.
307 Such effect is detrimental to the photocatalysis effect and leads to the decrease of the
308 concentration/formation of reactive excited state of decatungstate, namely, $\text{W}_{10}\text{O}_{32}^{4*}$.

309

310 **3.6. Effect of different initial pH**

311 The initial pH of the solution is a crucial parameter for the photocatalysis processes owing to
312 the stability of decatungstate and/or the various forms of the pollutants when a
313 protonation-deprotonation process is present (**Figure S4**). Thus, we studied the optimum pH under
314 our experimental conditions. For both substrates, SSZ and SPD at a concentration of 50.0 μM , the
315 excitation of decatungstate (40 μM) at 365 nm in the presence of 1.0 mM H_2O_2 permitted the
316 degradation of the pollutants with a rate that decreases when the pH of the solution increases. The
317 initial rates of SSZ were estimated to $2.1 \times 10^{-7} \text{ M min}^{-1}$ and $1.1 \times 10^{-7} \text{ M min}^{-1}$ at $\text{pH} = 3.0$ and 6.0
318 respectively and the initial rates of SPD were estimated to $7.4 \times 10^{-7} \text{ M min}^{-1}$ and $5.5 \times 10^{-7} \text{ M min}^{-1}$ at
319 $\text{pH} = 3.0$ and 6.0 respectively. This effect is more likely due to the fact that decatungstate is relatively
320 instable at high pH values as largely reported in the literature [29, 36].

321

322 **3.7. Elucidation of the initial products and degradation pathways for the pollutant** 323 **disappearance**

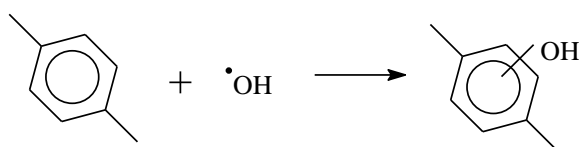
324 The elucidation of the generated byproducts was performed by employing HPLC/MS technique.

325 The results are gathered in **Table 2** for both substrates: SSZ and SPD. They were obtained for
326 irradiated samples that show roughly 30% conversion corresponding under our experimental
327 conditions to 120 min of irradiation time. The suggested structures were based on the elemental
328 compositions that were obtained from the obtained accurate masses. Some of them are clearly
329 primary products while others originate from secondary reactions.

330 The analysis of the chemical structures of the products leads us to the conclusion that in the early
331 stages of the irradiation mainly three and common chemical processes are involved for both
332 pollutants: i) hydroxylation ii) desulfurization and iii) scission at the azo group -N=N-.

333 The hydroxylation process is a clear evidence of the reactivity of the hydroxyl radical with the used
334 pollutants via an electron transfer process with the aromatic groups as largely reported in the
335 literature [37-39] leading finally to the addition of the hydroxyl group to the substrate (**scheme 3**).

336



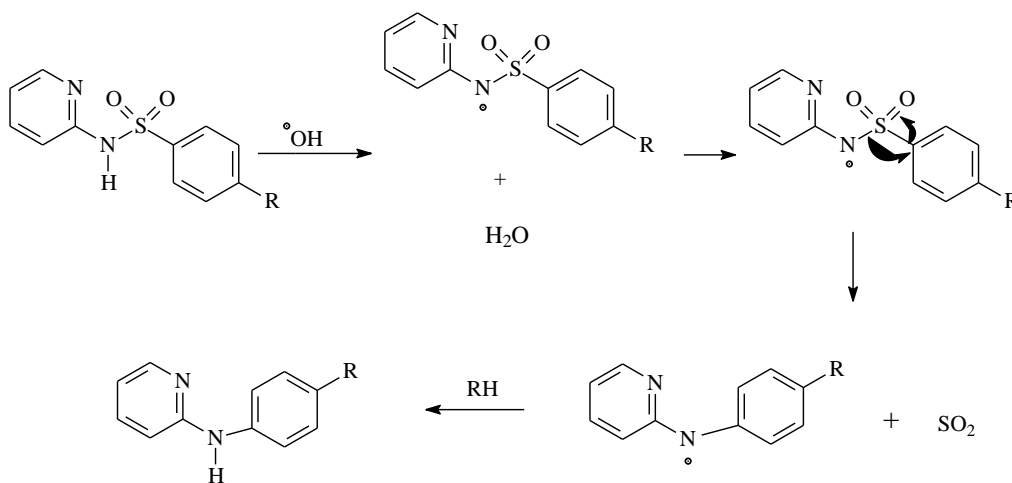
337

338

339 **Scheme 3:** Process of the reactivity of the hydroxyl radical with the benzene ring via an electron
340 transfer process

341

342 The desulfurization reaction is a reaction that is more likely triggered by the attack of the
343 hydroxyl radical on the adjacent amine group via an electron or/and a hydrogen abstraction process
344 followed by an intramolecular rearrangement as shown in the following **scheme 4** [40].

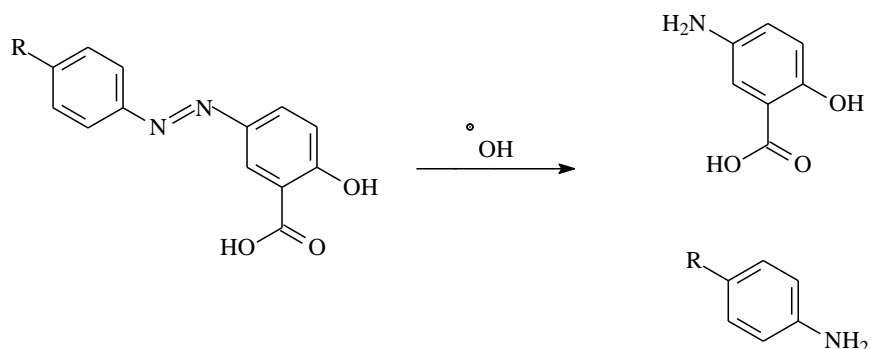


345

346 **Scheme 4:** The process of the desulfurization via an electron or/and a hydrogen abstraction process.

347

348 The third process is a scission at the azo group -N=N- that is more likely triggered by the attack
349 of the hydroxyl radical on the nitrogen sites leading to the formation of the two amine products as
350 shown in the following **scheme 5** [41]



351

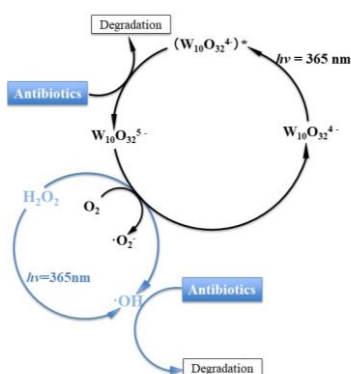
352

353 **Scheme 5:** Process of the azo group -N=N- scission via an attack of hydroxyl radical.

354

355 The photocatalytic process; involving decatungstate and H₂O₂ is given in **Scheme 6**. W₁₀O₃₂⁴⁻
356 could be excited upon UVA (365 nm) irradiation to form the excited state W₁₀O₃₂^{4-*} which leads, via
357 an electron transfer process with the pollutant, to the formation of the reduced form of decatungstate
358 namely W₁₀O₃₂⁵⁻ and the radical cation of the pollutant. This process provides one of the degradation
359 pathways. The regeneration of the photocatalyst can operate in the presence of H₂O₂ and oxygen,
360 following the formation of the hydroxyl radicals and superoxide anion radicals respectively. The
361 former free radical is highly and efficiently involved in the oxidation of SPD and SSZ. And this
362 represents the second pathway of organic pollutant degradation.

363



364

365

366 **Scheme 6:** Photocatalytic cycle of decatungstate/H₂O₂ system showing the two ways for the

367 degradation of the organic pollutant and the production of hydroxyl radicals via Fenton like reaction
368 between $W_{10}O_{32}^{5-}$ and H_2O_2 .

369

370

371 **3.8. Total organic carbon analysis**

372 In order to confirm the efficient degradation of the pollutants and also of their metabolites up to
373 the mineralization of the solution, we followed the total organic carbon (TOC) under light excitation.
374 We followed the evolution of TOC in a solution of SPD or/and SSZ under similar conditions ($[W] =$
375 $40.0 \mu M$, $[H_2O_2] = 10.0 mM$, $pH = 4.0$). In this case, after 24 h of irradiation, 90% of the initial
376 organic carbon (SSZ alone) has been transformed into CO_2 (**Fig. 6**). After 48h of irradiation, 75% of
377 the initial organic carbon (SPD alone, SPD and SSZ) has been converted into CO_2 (**Fig. 6**). Such
378 observations confirm that the decatungstate/ H_2O_2 system could be used in order to completely
379 achieve the removal of SPD or/and SSZ and their byproducts from water. Moreover they suggest that
380 decatungstate/ H_2O_2 system could be applied to treat multiple pollutants in water under the optimized
381 experimental conditions.

382

383 **4. Conclusion**

384 The combination of $W_{10}O_{32}^{4-}/H_2O_2/h\nu$ at $pH=4.0$ permitted an efficient degradation of the
385 pollutants sulfasalazine and sulfapyridine. The process involves two ways of reaction for the
386 oxidation of the organic compounds i) an electron transfer reaction with the excited state of
387 decatungstate and ii) also the hydroxyl radical reactivity. HO^\bullet is formed from the Fenton like
388 reaction with the reduced species of decatungstate, $W_{10}O_{32}^{5-}$ and H_2O_2 . The latter process represents
389 under our experimental conditions the main process for the disappearance of the pollutants and it is
390 also a way for the regeneration of starting catalyst, decatungstate. The main primary reactions were
391 found to be hydroxylation, desulfurization and scission at the azo group $-N=N-$ moiety. For
392 prolonged irradiations, the mineralization of the solution was observed which highlights the point
393 that the conjunction of $W_{10}O_{32}^{4-}/H_2O_2$ and light represent an interesting AOP's system for water
394 depollution. Indeed, the two possible pathways for the oxidation of organic compounds in this
395 system are important asset for treating polluted waters leading us to the conclusion that this system
396 could be considered in the future as a promising process for the decontamination of water. As a

397 perspective of this work, the immobilization of the photocatalyst decatungstate on solid supports will
398 be a goal in order to recycle the photocatalyst after treatment.

399

400 **Acknowledgements**

401 Peng CHENG thanks the Chinese scholarship council for its financial support and thanks professor
402 Marcello Brigante, engineer Guillaume Voyard and PhD student Yara Arbid for their help in some of
403 the experiments.

404

405 **References**

- 406 [1] R. Laxminarayan, A. Duse, C. Wattal, A.K. Zaidi, H.F. Wertheim, N. Sumpradit, E. Vlieghe, G.L.
407 Hara, I.M. Gould, H. Goossens, Antibiotic resistance—the need for global solutions, *The Lancet*
408 *infectious diseases*, 13 (2013) 1057-1098.
- 409 [2] C. Ding, J. He, Effect of antibiotics in the environment on microbial populations, *Applied*
410 *microbiology and biotechnology*, 87 (2010) 925-941.
- 411 [3] M. Qiao, G.-G. Ying, A.C. Singer, Y.-G. Zhu, Review of antibiotic resistance in China and its
412 environment, *Environment international*, 110 (2018) 160-172.
- 413 [4] Lucilaine Valéria de Souza Santos, Alexandre Moreira Meireles, Liséte Celina Lange,
414 Degradation of antibiotics norfloxacin by Fenton, UV and UV/H₂O₂, *Journal of environmental*
415 *management*, 154 (2015) 8-12.
- 416 [5] D. Calamari, E. Zuccato, S. Castiglioni, R. Bagnati, R. Fanelli, Strategic survey of therapeutic
417 drugs in the rivers Po and Lambro in northern Italy, *Environ. Sci. Technol.*, 37 (7) (2003) 1241–1248.
- 418 [6] B.A. Cunha, Antibiotic side effects, *Medical Clinics of North America*, 85 (2001) 149-185.
- 419 [7] A. Sola, Abuse of antibiotics in perinatology: negative impact for health and the economy,
420 *NeoReviews*, 21 (2020) e559-e570.
- 421 [8] Q.-Q. Zhang, G.-G. Ying, C.-G. Pan, Y.-S. Liu, J.-L. Zhao, Comprehensive Evaluation of
422 Antibiotics Emission and Fate in the River Basins of China: Source Analysis, Multimedia Modeling,
423 and Linkage to Bacterial Resistance, *Environmental Science & Technology*, 49 (2015) 6772-6782.
- 424 [9] W. Xiong, Z. Zeng, X. Li, G. Zeng, R. Xiao, Z. Yang, Y. Zhou, C. Zhang, M. Cheng, L. Hu,
425 Multi-walled carbon nanotube/amino-functionalized MIL-53 (Fe) composites: remarkable adsorptive
426 removal of antibiotics from aqueous solutions, *Chemosphere*, 210 (2018) 1061-1069.
- 427 [10] T. Oppenländer, *Photochemical purification of water and air: advanced oxidation processes*
428 *(AOPs)-principles, reaction mechanisms, reactor concepts*, John Wiley & Sons, 2007.
- 429 [11] L. Hu, P. Wang, T. Shen, Q. Wang, X. Wang, P. Xu, Q. Zheng, G. Zhang, The application of
430 microwaves in sulfate radical-based advanced oxidation processes for environmental remediation: A
431 review, *Science of The Total Environment*, (2020) 137831.
- 432 [12] J. Deng, Y. Shao, N. Gao, Y. Deng, S. Zhou, X. Hu, Thermally activated persulfate (TAP)
433 oxidation of antiepileptic drug carbamazepine in water, *Chemical Engineering Journal*, 228 (2013)
434 765-771.
- 435 [13] F. Sopaj, N. Oturan, J. Pinson, F.I. Podvorica, M.A. Oturan, Effect of cathode material on
436 electro-Fenton process efficiency for electrocatalytic mineralization of the antibiotic sulfamethazine,

437 Chemical Engineering Journal, 384 (2020) 123249.

438 [14] L. Hou, H. Zhang, X. Xue, Ultrasound enhanced heterogeneous activation of peroxydisulfate by
439 magnetite catalyst for the degradation of tetracycline in water, Separation and Purification
440 Technology, 84 (2012) 147-152.

441 [15] M. Xing, W. Xu, C. Dong, Y. Bai, J. Zeng, Y. Zhou, J. Zhang, Y. Yin, Metal sulfides as excellent
442 co-catalysts for H₂O₂ decomposition in advanced oxidation processes, Chem, 4 (2018) 1359-1372.

443 [16] C. Tanielian, Decatungstate photocatalysis, Coordination Chemistry Reviews, 178-180 (1998)
444 1165-1181.

445 [17] I. Texier, J.A. Delaire, C. Giannotti, Reactivity of the charge transfer excited state of sodium
446 decatungstate at the nanosecond time scale, Physical Chemistry Chemical Physics, 2 (2000)
447 1205-1212.

448 [18] M.D. Tzirakis, I.N. Lykakis, M. Orfanopoulos, Decatungstate as an efficient photocatalyst in
449 organic chemistry, Chemical Society Reviews, 38 (2009) 2609-2621.

450 [19] A. Allaoui, M.A. Malouki, P. Wong-Wah-Chung, Homogeneous photodegradation study of
451 2-mercaptobenzothiazole photocatalysed by sodium decatungstate salts: Kinetics and mechanistic
452 pathways, Journal of Photochemistry and Photobiology A: Chemistry, 212 (2010) 153-160.

453 [20] D.C. Duncan, T.L. Netzel, C.L. Hill, Early-Time Dynamics and Reactivity of Polyoxometalate
454 Excited States. Identification of a Short-Lived LMCT Excited State and a Reactive Long-Lived
455 Charge-Transfer Intermediate following Picosecond Flash Excitation of [W₁₀O₃₂]⁴⁻ in Acetonitrile,
456 Inorganic Chemistry, 34 (1995) 4640-4646.

457 [21] H.-Y. He, J. Lu, Highly photocatalytic activities of magnetically separable reduced graphene
458 oxide-CoFe₂O₄ hybrid nanostructures in dye photodegradation, Separation and Purification
459 Technology, 172 (2017) 374-381.

460 [22] H.-Y. He, Z. He, Q. Shen, Efficient hydrogen evolution catalytic activity of graphene/metallic
461 MoS₂ nanosheet heterostructures synthesized by a one-step hydrothermal process, International
462 Journal of Hydrogen Energy, 43 (2018) 21835-21843.

463 [23] M. Bonchio, M. Carraro, M. Gardan, G. Scorrano, E. Drioli, E. Fontananova, Hybrid
464 photocatalytic membranes embedding decatungstate for heterogeneous photooxygenation, Topics in
465 Catalysis, 40 (2006) 133-140.

466 [24] Y. Guo, C. Hu, X. Wang, Y. Wang, E. Wang, Y. Zou, H. Ding, S. Feng, Microporous
467 Decatungstates: Synthesis and Photochemical Behavior, Chemistry of Materials, 13 (2001)
468 4058-4064.

469 [25] Y. Nosaka, T. Takei, N. Fujii, Photoinduced reduction of W₁₀O₃₂⁴⁻ by organic compounds in
470 aqueous solution, Journal of Photochemistry and Photobiology A: Chemistry, 92 (1995) 173-179.

471 [26] C. Tanielian, R. Seghrouchni, C. Schweitzer, Decatungstate photocatalyzed electron-transfer
472 reactions of alkenes. Interception of the geminate radical ion pair by oxygen, The Journal of Physical
473 Chemistry A, 107 (2003) 1102-1111.

474 [27] S. Rafqah, P.W.-W. Chung, C. Forano, M. Sarakha, Photocatalytic degradation of metsulfuron
475 methyl in aqueous solution by decatungstate anions, Journal of Photochemistry and Photobiology A:
476 Chemistry, 199 (2008) 297-302.

477 [28] T. Charbouillot, M. Brigante, G. Mailhot, P.R. Maddigapu, C. Minero, D. Vione, Performance
478 and selectivity of the terephthalic acid probe for OH as a function of temperature, pH and
479 composition of atmospherically relevant aqueous media, Journal of Photochemistry and
480 Photobiology A: Chemistry, 222 (2011) 70-76.

- 481 [29] B.H. Bielski, Reevaluation of the spectral and kinetic properties of HO₂ and O₂⁻ free radicals,
482 Photochemistry and Photobiology, 28 (1978) 645-649.
- 483 [30] L. Wu, X. Zhang, H. Ju, Amperometric glucose sensor based on catalytic reduction of dissolved
484 oxygen at soluble carbon nanofiber, Biosensors and Bioelectronics, 23 (2007) 479-484.
- 485 [31] H. Ju, C. Shen, Electrocatalytic reduction and determination of dissolved oxygen at a poly (nile
486 blue) modified electrode, Electroanalysis: An International Journal Devoted to Fundamental and
487 Practical Aspects of Electroanalysis, 13 (2001) 789-793.
- 488 [32] Y.-S. Shen, Y. Ku, K.-C. Lee, The effect of light absorbance on the decomposition of
489 chlorophenols by ultraviolet radiation and UV/H₂O₂ processes, Water research, 29 (1995) 907-914.
- 490 [33] G.S. Wang, C.H. Liao, H.W. Chen, H.C. Yang, Characteristics of Natural Organic Matter
491 Degradation in Water by UV/H₂O₂ Treatment, Environmental Technology, 27 (2006) 277-287.
- 492 [34] H. Christensen, K. Sehested, H. Corfitzen, Reactions of hydroxyl radicals with hydrogen
493 peroxide at ambient and elevated temperatures, The Journal of Physical Chemistry, 86 (1982)
494 1588-1590.
- 495 [35] M. Alam, M. Kelm, B. Rao, E. Janata, Reaction of H with H₂O₂ as observed by optical
496 absorption of perhydroxyl radicals or aliphatic alcohol radicals and of OH with H₂O₂. A pulse
497 radiolysis study, Radiation Physics and Chemistry, 71 (2004) 1087-1093.
- 498 [36] E. Papaconstantinou, A. Hiskia, A. Troupis, Photocatalytic processes with tungsten oxygen
499 anion clusters, Frontiers in Bioscience, 8 (2003) s813-825.
- 500 [37] A. Broo, S. Larsson, Electron transfer in azurin and the role of aromatic side groups of the
501 protein, The Journal of Physical Chemistry, 95 (1991) 4925-4928.
- 502 [38] J. Howell, J. Goncalves, C. Amatore, L. Klasinc, R. Wightman, J. Kochi, Electron transfer from
503 aromatic hydrocarbons and their. pi.-complexes with metals. Comparison of the standard oxidation
504 potentials and vertical ionization potentials, Journal of the American Chemical Society, 106 (1984)
505 3968-3976.
- 506 [39] B. Krimmel, F. Swoboda, S. Solar, G. Reznicek, OH-radical induced degradation of
507 hydroxybenzoic-and hydroxycinnamic acids and formation of aromatic products—a gamma
508 radiolysis study, Radiation Physics and Chemistry, 79 (2010) 1247-1254.
- 509 [40] Y.-q. Zhang, X.-f. Xie, W.-l. Huang, S.-b. Huang, Degradation of aniline by Fe²⁺-activated
510 persulfate oxidation at ambient temperature, Journal of Central South University, 20 (2013)
511 1010-1014.
- 512 [41] A. Rehorek, M. Tauber, G. Gübitz, Application of power ultrasound for azo dye degradation,
513 Ultrasonics Sonochemistry, 11 (2004) 177-182.

514

515

Figure captions:

516
517
518
519
520
521
522
523
524
525
526
527
528
529
530
531
532
533
534
535
536
537
538
539

Figure 1: Emission spectrum of lamps used in the reactor and UV-visible absorption spectra of SSZ, SPD and decatungstate (W)

Figure 2: Degradation kinetics of (A) SSZ and (B) SPD in the different systems. [SSZ] = [SPD] = 50 μ M; [H₂O₂] = 1 mM; [W] = 40 μ M; pH = 4.0

Figure 3: Formation of Hydroxyterephthalic acid by excitation of decatungstate (40 μ M) at 365 nm in the presence of hydrogen peroxide (1 Mm) and terephthalic acid (50 μ M) as a function of irradiation time at pH = 4.0

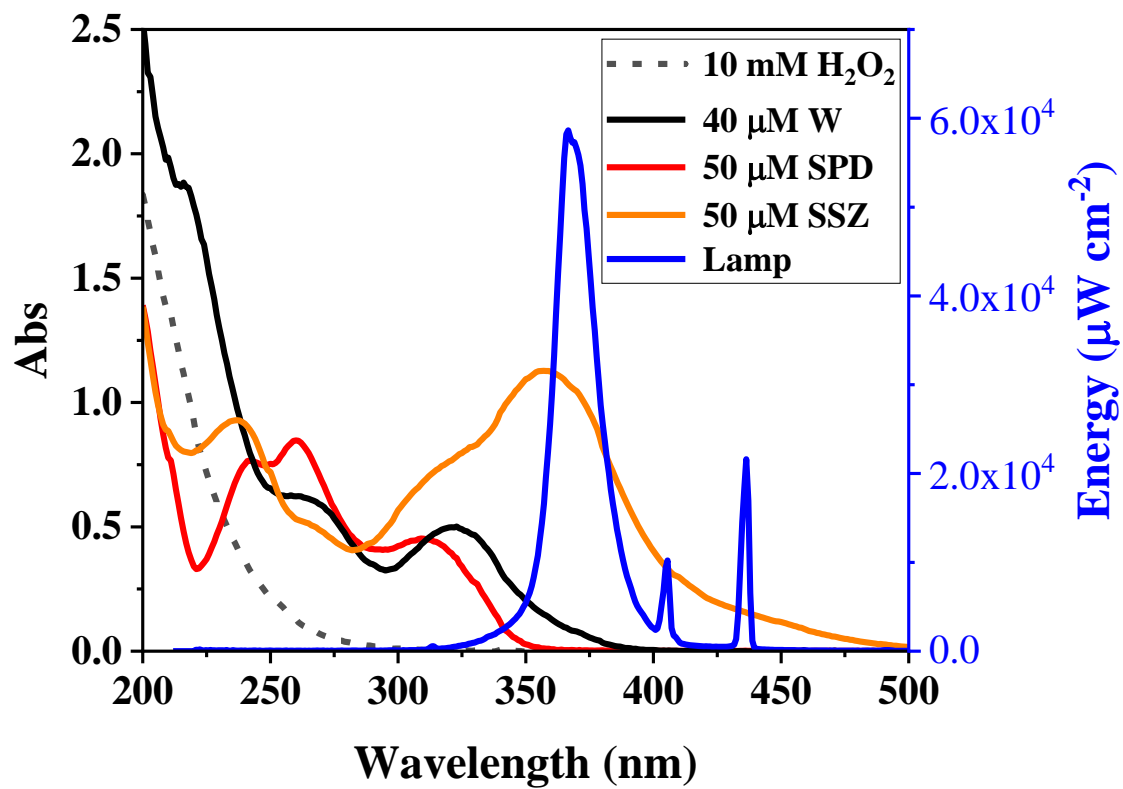
Figure 4: Effect of decatungstate concentration on SSZ (A) and SPD (B) removal in the presence of hydrogen peroxide. [SSZ] = [SPD] = 50 μ M; [H₂O₂] = 10 mM, pH = 4.0

Figure 5: Initial degradation rates of SSZ and SPD as a function of their initial concentrations. [H₂O₂] = 10 mM; [W] = 40 μ M; pH = 4.0

Figure 6: Evolution of TOC in a SSZ or/and SPD solution in decatungstate/H₂O₂ system. [H₂O₂] = 10 mM; [W] = 40 μ M; pH = 4.0

540

Figure 1



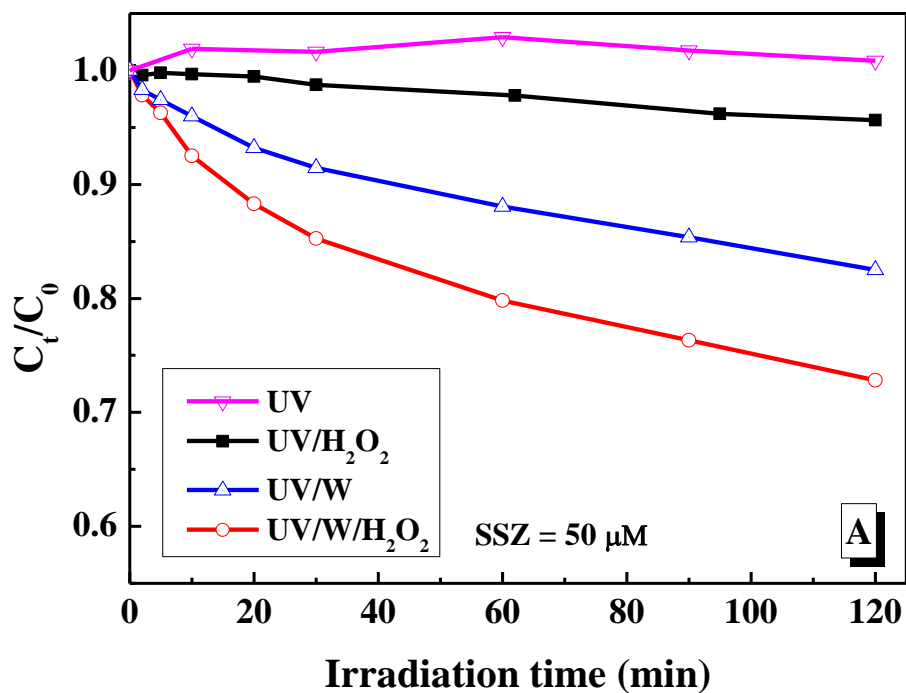
541

542

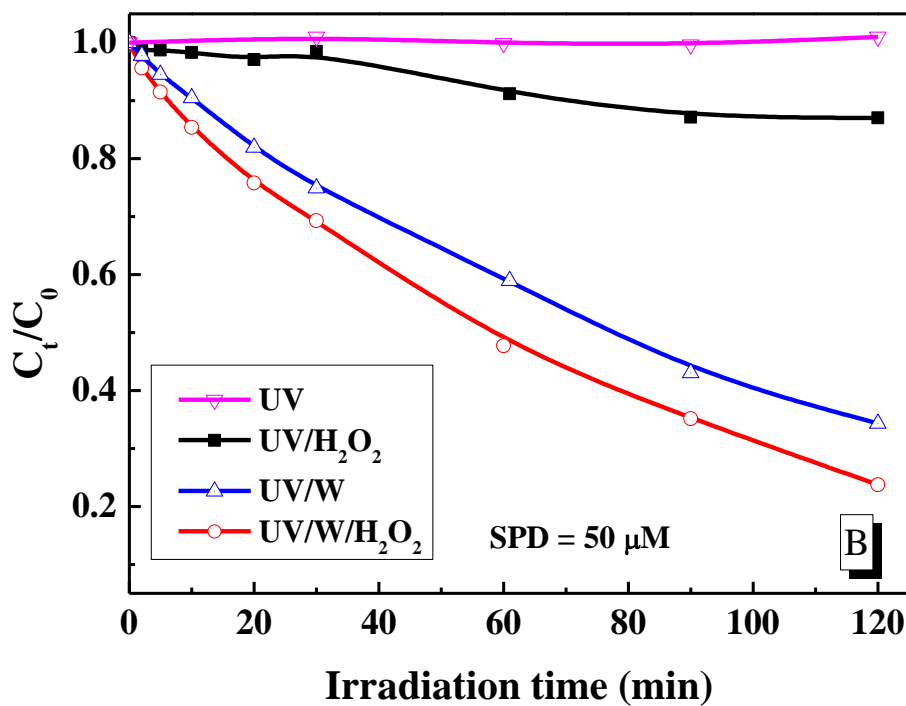
543

544
545

Figure 2



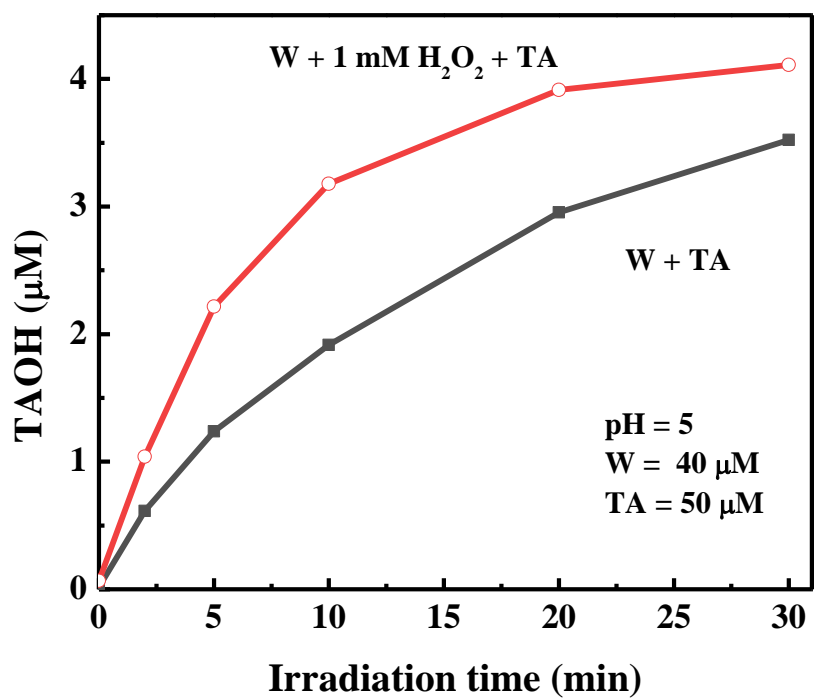
546



547
548
549

550
551

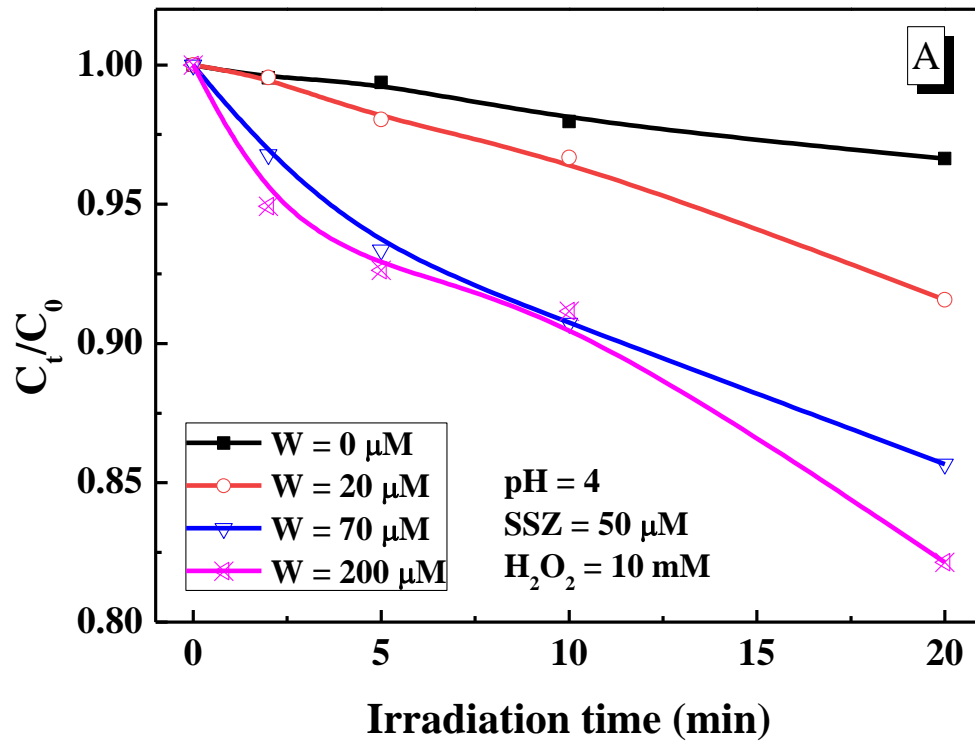
Figure 3:



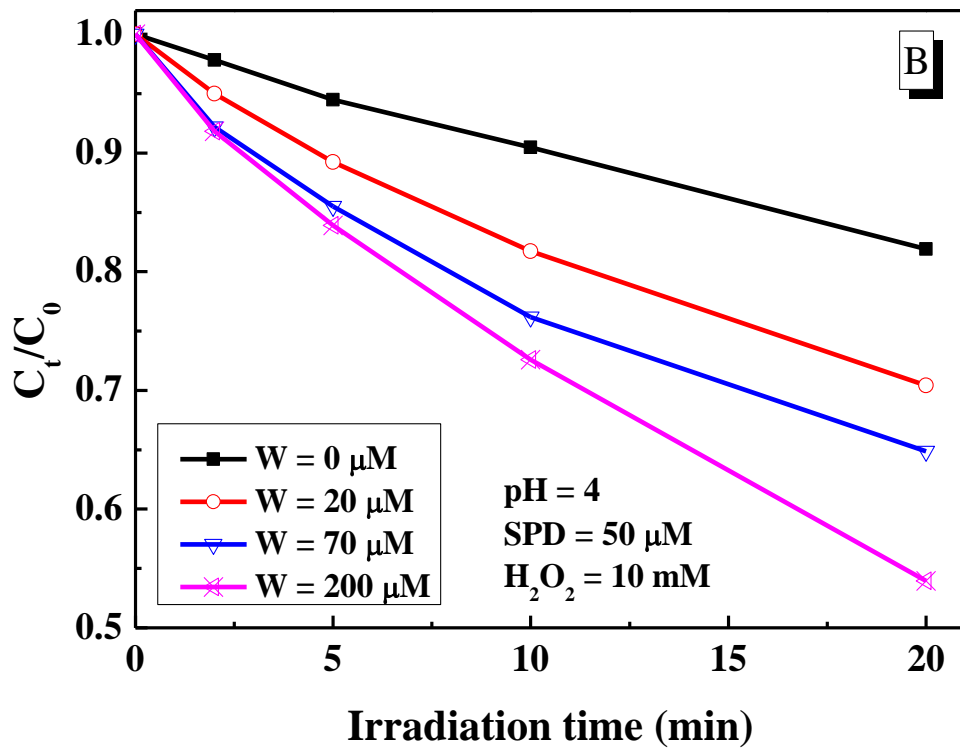
552
553
554

555
556

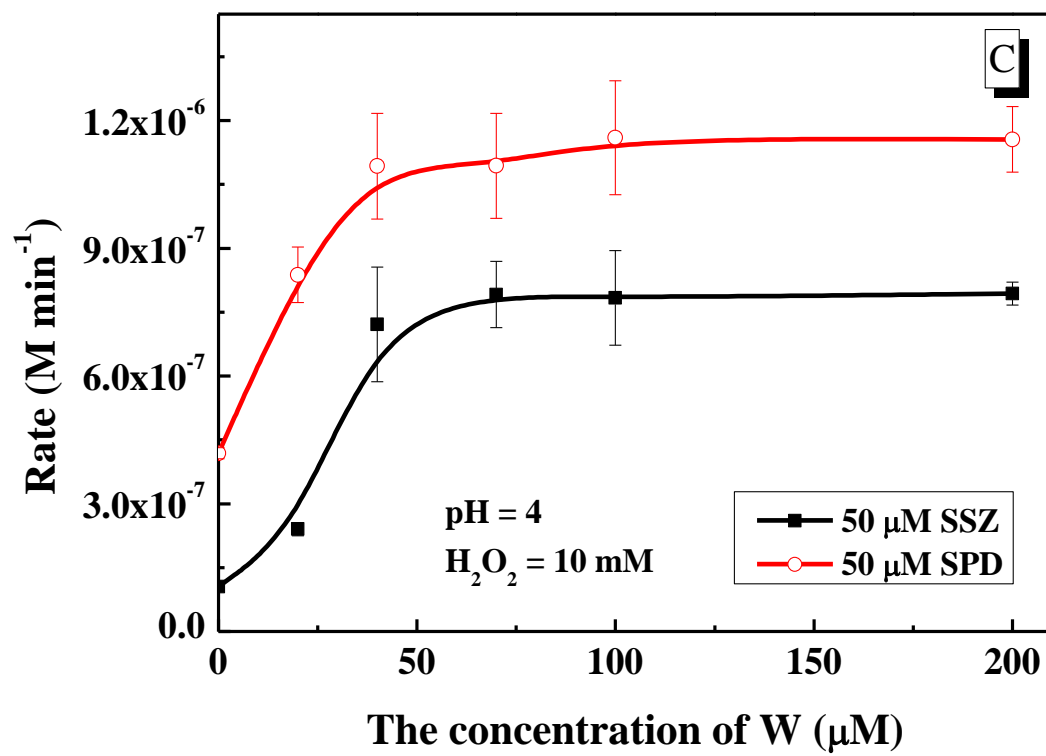
Figure 4



557



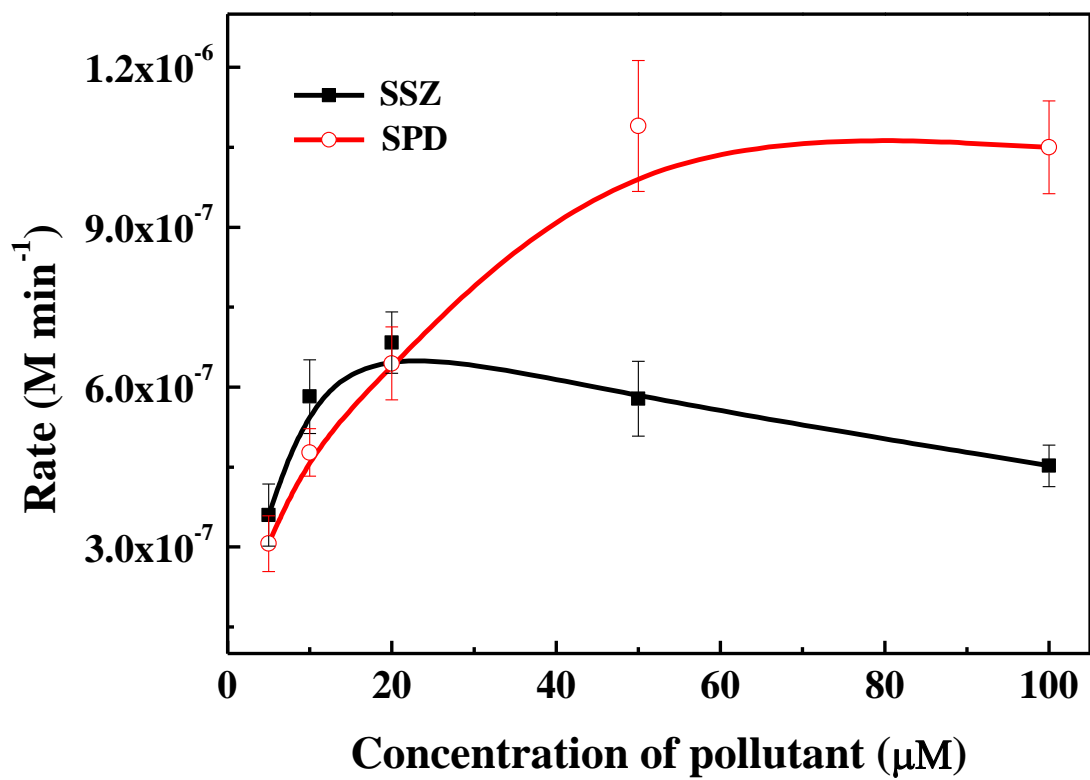
558



559
560
561

562

Figure 5:

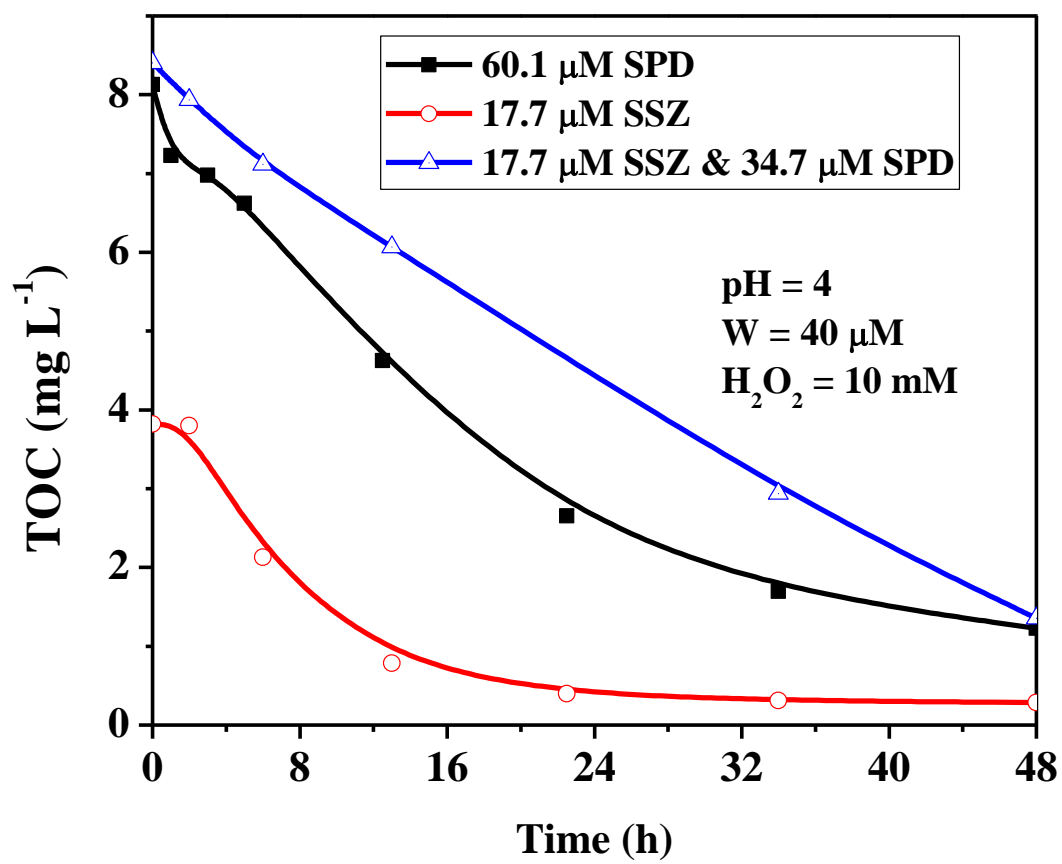


563

564

565

Figure 6:



569 Table 1: SSZ and SPD initial degradation rates as a function of H₂O₂ concentration. [W] = 40 μM;
 570 [SSZ] = [SPD] = 50 μM; pH = 4.0.
 571

[H ₂ O ₂] mM	Initial rate of SSZ disappearance M min ⁻¹		Initial rate of SPD disappearance M min ⁻¹	
	Without decatungstate	With decatungstate	Without decatungstate	With decatungstate
	0	No degradation	1.2×10 ⁻⁷	No degradation
1	0.1×10 ⁻⁷	1.6×10 ⁻⁷	0.6×10 ⁻⁷	7.0×10 ⁻⁷
10	1.1×10 ⁻⁷	6.1×10 ⁻⁷	4.2×10 ⁻⁷	10.9×10 ⁻⁷
50	5.0×10 ⁻⁷	14.0×10 ⁻⁷	13.7×10 ⁻⁷	21.9×10 ⁻⁷
100	7.2×10 ⁻⁷	21.5×10 ⁻⁷	21.3×10 ⁻⁷	33.9×10 ⁻⁷

572

573

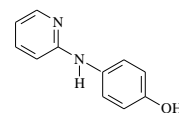
574

575
576
577

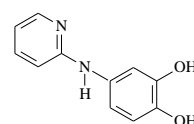
Table 2: MS analysis of SPD and SSZ by-products and suggested structures. [W] = 40 μ M; [H₂O₂] = 10 mM; [SSZ] = [SPD] = 50 μ M; pH = 4.0.

SSZ			SPD		
m/z	Elemental composition	Suggested structure	m/z	Elemental composition	Suggested structure
398	C ₁₈ H ₁₄ N ₄ O ₅ S		249	C ₁₁ H ₁₁ N ₃ O ₂ S	
414	C ₁₈ H ₁₄ N ₄ O ₆ S		250	C ₁₁ H ₁₀ N ₂ O ₃ S	
334	C ₁₈ H ₁₄ N ₄ O ₃		281	C ₁₁ H ₁₁ N ₃ O ₄ S	
249	C ₁₁ H ₁₁ N ₃ O ₂ S		265	C ₁₁ H ₁₁ N ₃ O ₃ S	
250	C ₁₁ H ₁₀ N ₂ O ₃ S		263	C ₁₁ H ₉ N ₃ O ₃ S	
186	C ₁₁ H ₁₀ N ₂ O		279	C ₁₁ H ₉ N ₃ O ₄ S	
202	C ₁₁ H ₁₀ N ₂ O ₂		266	C ₁₁ H ₁₀ N ₂ O ₄ S	
266	C ₁₁ H ₁₀ N ₂ O ₄ S		185	C ₁₁ H ₁₁ N ₃	

186 **C₁₁H₁₀N₂O**



202 **C₁₁H₁₀N₂O₂**



578

579